COMPARING NET SURFACE RADIATION ESTIMATION FROM REMOTE SENSING TO FIELD DATA

FOLHES, M. T.[1]; RENNÓ, C. D.[2]; SOARES, J. V.[2]; SILVA, B. B.[3]

ABSTRACT: Distribution of regional net radiation flux density over an irrigated agricultural area was analysed using a method that combine satellite remote sensing with field observation. Measurement of net radiation was collected over an irrigated banana field. Using the net radiation submodel implemented in METRIC in combination with TM/Landsat image, the radiant fluxes were calculated for each pixel within the study area. Thereafter, a comparison is made between the fluxes measured by instruments and estimated by the method. It was shown that the used model provided net surface radiation estimate close to the field measurement, with a relative error less than 0.03.
KEYWORDS: Metric; net surface radiation; remote sensing.

1. INTRODUCTION: Net surface radiation density flux (R_n) is a key variable for computing evapotranspiration and is a driving force in many other physical and biological processes Experimentally, instruments such as pyranometers for shortwave radiation and pyrgeometers for longwave provide the point measurement of radiant fluxes. Nevertheless, the needs of the modeling community to provide the R_n on a regional scale have stimulated the development of using remote sensing data. Remote sensing estimates of R_n provide a means to assess, in a spatially distributed manner, exchange processes of water and heat over the land surface (Bastiaanssen et al., 1998).

The R_n submodel implemented in METRIC^{TM} (Mapping Evapotranspiration at High Resolution and with Internalized Calibration) was employed here to calculate the R_n over the study area based on satellite data. An image-processing model for calculating evapotranspiration as a residual of the surface energy balance, METRIC has been applied in the U.S.A with Landsat images to predict monthly and seasonal evapotranspiration for water rights accounting and for operation of ground water models (Allen et al., 2005; Tasumi et al., 2005).

In the present investigation, the purpose was to evaluate the submodel to estimate the radiation balance components over an irrigated agricultural area combining satellite remote sensing data with field observations. Thus, a field campaign has been held in the Apodi plain, in the Brazilian semi-arid region, via a collaborating study between the National Institute for Space Research and the Federal University of Campina Grande. A unique database has been collected since august 2005, including field measurements of surface properties and meteorological variables. Such database will provide the opportunity to refine remote sensing actual evapotranspiration estimation models accuracy.

2. DATA AND METHOD:

2.1 Study Area: The study was carried out in an agricultural area in the Apodi plain, northeastern Brazil (S 05°10', W 37° 53', 130 m above sea level) (Figure 1). The Apodi plain has a semi-arid climate with annual precipitation of 772 mm. The agriculture relies on irrigation from the Jaguaribe River. The area was selected on the basis of availability of ground reference data on net radiation.

2.2 Remote Sensing and Meteorological Data: The used data consisted of one TM/Landsat-5 scene (WRS path 216 row 64) acquired over the Apodi plain on October 24 2005. This date had propitious weather conditions and clouds were not present. Digital elevation model from Shuttle Radar Topographic Mission (SRTM) for the study area provided the altitude data. Data from a meteorological station were available to evaluate the calculation of the components of the radiation

[1] CAPES fellow, INPE, Av. dos Astronautas, 1758, CEP 12227-010, São José dos Campos, SP. Tel.: 12-3945-6732. E-mail: folhes@ltid.inpe.br
[2] Researcher, Dr., National Institute for Space Research (INPE).
[3] Researcher, Dr., Federal University of Campina Grande.

balance. The station was installed temporarily for the duration of the experiment at a banana field (lat: 05°04'40''S; long: 37°51'29''W). The meteorological data consist of 10-minute period averaging of measured incoming and outgoing solar radiation and incoming and outgoing thermal radiation.

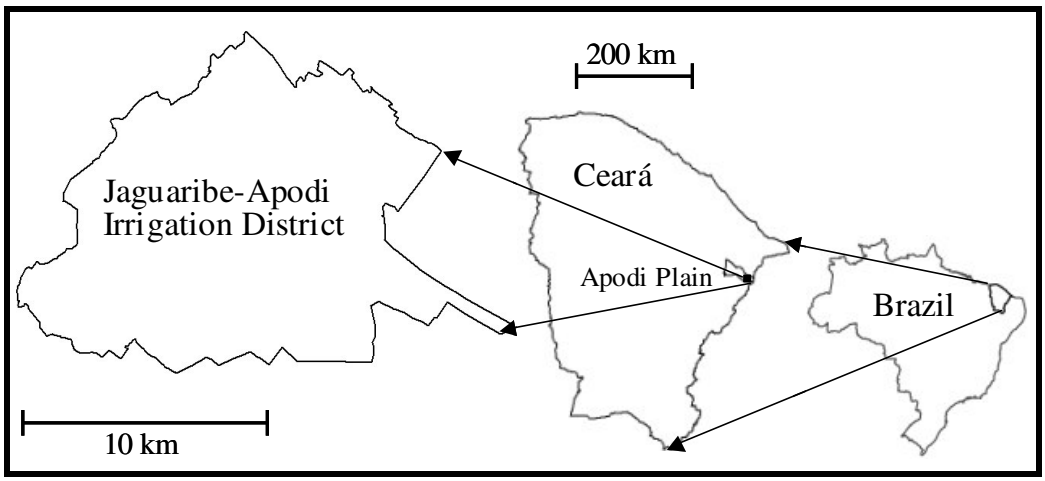

Figure 1: The study area in national and regional context.

2.3 Net Radiation Flux Estimation Model: Computed from the land surface radiation balance as:

$$R_n = (1-\alpha)R_{iS} + R_{iL} - R_{oL} - R_{iL}(1-\varepsilon_s)$$

where R_n is instantaneous net surface radiation (W/m^2); R_{iS} is instantaneous incoming shortwave solar radiation (W/m^2); R_{iL} and R_{oL} are instantaneous incoming and outgoing longwave radiation (W/m^2); α is surface albedo; ε_s is broad-band surface emissivity.

2.3.1 Surface Albedo (α): It was determined by integrating spectral reflectances in the shortwave bands of the TM/Landsat image (Tasumi and Allen, 2006). Therefore, surface albedo is calculated as:

$$\alpha = \sum_{i=1}^{6}(r_{s,i} \times w_i)$$

where $r_{s,i}$ is the at-surface reflectance for band i; w_i is a weighting coefficient representing the at-surface solar radiation fraction occurring within the spectral range of band i:

$$W_i = \frac{\int_{LOi}^{UPi} R_s^{\downarrow} \cdot d\lambda}{\int_{0.3}^{4.0} R_s^{\downarrow} \cdot d\lambda}$$

where UP_i and LO_i are upper and lower wavelength (μm) bounds assigned to TM band i; 0.3 to 4.0 (μm) are the endpoints of solar radiation integration.

The $r_{s,i}$ is derived by correcting the at-satellite band reflectance for back-scattering and atmospheric transmittance:

$$r_{s,i} = \frac{r_{t,i} - r_{a,i}}{\tau_{in,i} \times \tau_{out,i}}$$

where $\tau_{in,i}$ and $\tau_{out,i}$ are atmospheric transmittances for incoming and reflected solar radiation for band i; $r_{t,i}$ is at-satellite reflectance for band i; $r_{a,i}$ is atmospheric path reflectance for band i.

The $r_{t,i}$ is computed using the following equation given for Landsat images:

$$r_{t,i} = \frac{\pi \times L_i}{E_i \times cos(\theta) \times d_r}$$

where L_i is at-satellite spectral radiance (W.m^{-2}.ster^{-1}.μm^{-1}); E_i is the mean solar exoatmospheric radiation for band i (W.m^{-2}. μm^{-1}); θ is the solar incident angle; and d_r is the Earth-Sun distance in astronomical units.

Given relative humidity measurements at the 10-minute time step available from the weather station, the atmospheric transmittance functions for τ_{in} and τ_{out} are determined as:

$$\tau_{in,i} = c_1 \times exp\left[\frac{c_2 P_{ar} - c_3 W - c_4}{cos\,\theta}\right] + c_5$$

where P_{ar} is atmospheric pressure (kPa); θ is the solar incident angle for horizontal surfaces; W is precipitable water in the atmosphere (mm); and c_1 to c_5 are fitted satellite-dependent constants presented in the Tasumi and Allen (2006) work:

$$\tau_{out,i} = c_1 \times exp\left[\frac{c_2 P_{ar} - c_3 W - c_4}{cos\,\eta}\right] + c_5$$

where η is the sensor view angle.

The back-scattering term is finally determined as:

$$r_{a,i} = c_i \times (1 - \tau_{in,i})$$

2.3.2 Incoming Shortwave Radiation (R_{iS}): In the following equation, R_{iS} is predicted, assuming cloud-free and relatively dry conditions:

$$R_{iS} = G_{cs} \times cos\,\theta \times d_r \times \tau_{in}$$

where G_{cs} is the solar constant (1367 W.m^{-2}); θ is the solar incident angle; and τ_{in} is the broad-band incoming atmospheric transmittance.

The τ_{in} can be estimated using an elevation-based relationship from Allen et al. (1998):

$$\tau_{in} = 0.75 \times 2 \times 10^{5} \times z$$

where z is the elevation above sea level (m), taken from the available SRTM-90m data.

2.3.3 Incoming Longwave Radiation (R_{iL}): R_{iL} is calculated by the following equation from Bastiaanssen et al. (1998) for clear-sky conditions:

$$R_{iL} = 1.08 \times (-ln\,\tau_{sw})^{0.265} \times \theta \times Ta^4$$

where Ta is the surface temperature at a reference point, generally select to be a well-watered pixel so that surface temperature and air temperature are similar.

2.3.4 Outgoing Longwave Radiation (R_{oL}): Since R_{oL} is the thermal radiation flux emitted from the Earth's surface to the atmosphere, it is calculated by applying Stefan-Boltzman equation:

$$R_{oL} = \varepsilon_s \times \theta \times T_s^4$$

where ε_s is the broadband surface emissivity (4 to 50 μm) (dimensionless) and T_s is the surface radiometric temperature (K).

Surface emissivity is estimated using NDVI and an empirically derived method from Van de Griend and Owe (1993):

$$\varepsilon_s = 1.009 + 0.047\, ln(NDVI)$$

where NDVI is Normalized Difference Vegetation Index computed using reflectance of band 3 and 4.

The T_s is computed using the following modified Plank equation:

$$T_s = \frac{1260.56}{ln\left(\frac{\varepsilon_o 607.76}{L_6} + 1\right)}$$

where L_6 is the thermal radiance from the surface in spectral range of band 6 ($W.m^{-2}.ster^{-1}.\mu m^{-1}$); ε_o is the narrow band thermal infrared surface emissivity (dimensionless).

The thermal radiance from the surface is calculated following Wukelic et al. (1989) as:

$$L_6 = (DN \times 0.0056322) + 0.1238$$

where DN is the digital number of each pixel of the thermal band.

2.4 Method of Verification: Due to uncertainty concerning the georegistration of the TM imagery, R_n estimates were taken from spatial average of retrievals within a 3 x 3 pixel window centered on the experimental site. The relative error (RE) can quantitatively measure the difference between the derived results and measured values as:

$$RE = 100.\left(\frac{\text{absolute error}}{\text{measured value}}\right)$$

3. RESULTS AND DISCUSSION: The derived R_n for the area is in good accordance with the land cover types, and they show a wide range due to the strong contrast of surface features in the area. Net radiation ranged from 205 to 1010 $W.m^{-2}$. The red-brown areas in Figure 2, which form most of the resulted R_n map, are mainly drier sparse small woods and rather extensive bare soil; the upper and left areas (red colored) correspond to a degraded area, in which we can find mainly sparsely distributed brushwood; areas in green are primary small fields of irrigated crops and fruit trees, and dense dry forest; and the blue areas mark watery surfaces.

The last step of this study was the validation of the components of the radiation balance calculated by the model. An overview of the results is given in Table 1. Accordingly, the method might underpredict incoming and outgoing longwave radiation, which largely offsets the overestimated incoming and outgoing shortwave radiation, inducing error compensation. The combinations of several factors could explain the error on model estimates, i.e. the uncertainties on the estimates of surface emissivity, atmospheric transmittance, surface and air temperature, as well as instrumental error.

However, the difference between the derived R_n and the field measurement at the same time as Landsat observation, 09:30 local time, is less than 3%. It was shown that the model provided R_n estimate close to the field measurement, with an absolute error of 14 $W.m^{-2}$. Such an error was low as compared to results reported in previous studies when considering similar approaches (Wang et al., 1995; Ma et al., 1999).

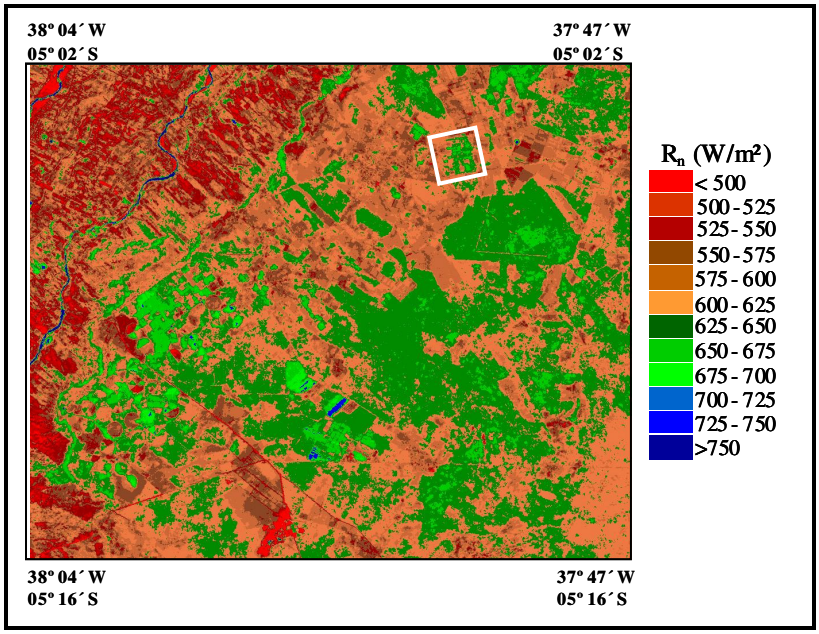

Figure 2 – The R_n map in the agro-ecosystem area. The inset represents the banana field investigated.

Table 1 – Basic instantaneous measurements and estimates of the components of the radiation balance

Parameter	Unit	Measured value	Estimated value	Absolute error ($W.m^{-2}$)	Relative Error (%)
Shortwave rad. incoming	$W.m^{-2}$	874	934	60	6.8
Shortwave rad. outgoing	$W.m^{-2}$	144	159	15	10.4
Longwave rad. incoming	$W.m^{-2}$	396	349	47	11.8
Longwave rad. outgoing	$W.m^{-2}$	494	474	20	4.0
Net radiation	$W.m^{-2}$	632	646	14	2.2

4. CONCLUSION: The METRIC R_n submodel described in this paper has been developed to combine remote sensing and field data to estimate net surface radiation flux. The algorithm was tested with ground-based radiant flux measurements collected in a banana field. Though very good agreement between both types of determination was observed, only a single value at a specific time of specific day is used in this research. To reach more accurate regional radiant fluxes densities, more field observations have to be used.

REFERENCES

Allen, R. G.; Pereira, L. S.; Raes, D. **Crop evapotranspiration**. Rome: FAO, 1998. 297p. (FAO. Irrigation and Drainage Paper 56).

Allen, R. G.; Tasumi. M.; Morse, A; Trezza, R. A Landsat-based energy balance and evapotranspiration model in Western US water rights regulation and planning. **Irrigation and Drainage Systems**, v. 19, p. 251-268, 2005.

Bastiaanssen, W. G. W; Pelgrum, H.; Wang, J.; Ma, Y.; Moreno, J.; Roerink, G. J.; van der Wal, T. A remote sensing surface energy balance algorithm for land (SEBAL): validation. **Journal of Hydrology**, v. 212/213, p. 213-229, 1998.

Ma, Y. Remote sensing parameterization of regional net radiation over heterogeneous land surface of Tibetan Plateau and arid area. **International Journal of Remote Sensing**, v. 24, n. 15, p. 3137-3148, 1999.

Tasumi. M.; Allen, R.G.; Trezza, R. At-surface and albedo from satellite for operational calculation of land surface. **Agricultural and Forest Meteorology**, 2006, sent.

Tasumi. M.; Trezza, R.; Allen, R. G.; Wright, J. L. Operational aspects of satellite-based energy balance models for irrigated crops in the semi-arid U.S. **Irrigation and Drainage Systems**, v. 19, p. 355–376, 2005.

Van de Griend, A. A.; Owe, M. On the relationship between thermal emissivity and the normalized difference vegetation index for natural surfaces. **International Journal of Remote Sensing,** v. 14, n. 6, p. 1119-1131, 1993.

Wukelic, G. E; Gibbons, D. E.; Martucci, L. M.; Foote, H. P. Radiometric calibration of Landsat mapper thermal band. **Remote Sensing of Environment**, v. 28, p. 339-347, 1989.

Wang, J.; Ma, Y.; Menenti, M.; Bastiaanssen, W. G. W.; Mitsuta, Y. The Scaling-up of Processes in the Heterogeneous Landscape of HEIFE with the Aid of Satellite Remote Sensing. **Journal of the Meteorological Society of Japan**, v. 73, n. 6, p. 1235-1244, 1995.